Evaluating of Noise Reduction Techniques for Turboengine Test Stands: A Preliminary Analysis

Laurentiu Cristea * and Marius Deaconu

Posted Date: 31 May 2024

doi: 10.20944/preprints202405.2135.v1

Keywords: baffle attenuator; turboengine stand; experimental validation; Embleton's method; anechoic chamber; rectangular duct flow.

 doi:10.20944/preprints202405.2135.v1

Article

Evaluating of Noise Reduction Techniques for Turboengine Test Stands: A Preliminary Analysis

Laurentiu Cristea * and Marius Deaconu

National Research and Development Institute for Gas Turbines COMOTI, 220D Iuliu Maniu, 061126 Bucharest, Romania; marius.deaconu@comoti.ro

* Correspondence: laurentiu.cristea@comoti.ro

Abstract: Emphasizing the importance of acoustic attenuation in maintaining compliance with stringent noise regulations and enhancing workplace safety, the analysis covers the theoretical and practical aspects of sound attenuation in a turboengine testing stand. This paper presents a preliminary analysis and also an evaluation of a procedure for projecting a noise attenuator for industrial application and especially for turboengine test stands. While primarily focusing on the static acoustic behavior of the attenuator, considerations were also made regarding flow dynamics, Mach number-dependent attenuation, pressure drop, and self-generated noise aspects to provide a comprehensive perspective in selecting the optimal design configuration. The study investigates different calculation methods for assessment of the noise reduction for linear and staggered baffles, applied on a scaled reduced model of attenuator. Thus, the critical parameters and projecting requirements necessary for effective noise reduction in high-performance turboengine testing environments will be evaluated in a down-scaled model. Key factors examined include the selection of design parameters and configurations from various options. Advanced computational methods, like analytic and finite element analysis (FEM) are utilized to predict the acoustic performance and identify potential design optimizations. Experimental validation is performed to corroborate the simulation results, ensuring the reliability and efficiency of the attenuator. The findings indicate that a well-designed sound attenuator module can significantly reduce noise levels without compromising the operational performance of the turboengine inside a test cell.

Keywords: baffle attenuator; turboengine stand; experimental validation; Embleton's method; anechoic chamber; rectangular duct flow

1. Introduction

Sound attenuators, commonly referred to as silencers, are integral to reducing acoustic emissions during turboengine testing. Their efficacy is influenced by various factors, including material properties, geometric configurations, and integration within the test stand infrastructure. Despite their significance, comprehensive studies systematically addressing the design and implementation requirements of these modules in turboengine testing environments are lacking. This study aims to address this gap by conducting a thorough preliminary analysis of sound attenuator modules. The objective is to establish a robust framework for the design and integration of sound attenuator modules, ensuring optimal acoustic performance while maintaining the operational integrity of turboengine test stands. This analysis encompasses both theoretical approaches and practical considerations, employing advanced simulation techniques such as finite element analysis to predict and enhance the acoustic attenuation capabilities of the proposed designs. Additionally, we conduct experimental validations to ensure the accuracy and reliability of our simulation results. By comparing theoretical predictions with empirical data, we identify key areas for design optimization and potential innovations in attenuator technology. This paper not only contributes to the fundamental knowledge of noise attenuation but also provides valuable insights for engineers and designers involved in the development of turboengine testing infrastructure. Designing an acoustic

 doi:10.20944/preprints202405.2135.v1

attenuator for a turboengine test stand involves utilizing analytical models based on empirical calculation relationships or advanced methods such as finite element simulations. Each approach has its advantages and disadvantages: analytical methods provide quick results but are prone to high error margins, whereas the finite element method offers greater accuracy but is time-consuming and resource-intensive. Both methods necessitate precise input data to ensure the accuracy of the predicted results.

Improving transmission loss through pipe wrappings and enclosure walls, as well as attenuating sound propagating in ducts, involves various strategies and materials aimed at reducing sound energy transmission through these structures, as studied by Bies and Hansen [1]. A broadband low-frequency rectangular silencer with a sandwich plate was experimentally tested by Wang et al. [2], achieving a transmission loss of more than 10 dB across the entire frequency band. The propagation of sound in rectangular ducts was analyzed in detail by Erkan [3] through mathematical analysis of sound propagation and radiation. A reactive perforated muffler was investigated numerically, experimentally, and analytically by Sumit et al. [4], resulting in transmission loss data. Various internal configurations for silencers, including the effects of side-branch partitions, multi-chamber partitions, and their combined effects, were examined by Yu and Cheng [5]. Pressure radiation from a perforated region was studied by Wang et al. [6], who found that such regions can significantly reduce the pressures radiated from a duct outlet. Numerical and experimental investigations were conducted by Zhou et al. [7], concluding that isotropic behavior was observed in perforated plates with circular holes under square and triangular penetration patterns. Low-frequency tonal noise reduction was studied by Williams et al. [8] using dissipative and reactive elements in silencers, enabling reactive elements to function effectively over an extended low to medium frequency range. Terashima [9] utilized a finite element approach to evaluate sound transmission loss in perforated silencers, concluding that discrepancies in sound transmission loss results may be attributed to the viscous effects of sound wave propagation and geometric imperfections. Kalita and Singh [10] performed an acoustic performance analysis of absorption materials used in sound attenuators, concluding that a type of glass wool (with a density of 24 kg/m^3 and flow resistivity of 14,000 Pa s/m^2) inserted in a muffler yielded the best transmission loss compared to rock wool, polyester, or melamine. Experiments with parallel baffled mufflers and perforated panels were conducted by Xiaowan [11], who created a testing stand and studied the transmission loss for various panel configurations. Liu et al. [12] investigated noise reduction and acoustic impedance of a duct intake using a modified time domain model instead of the classical transmission loss model. Porous lamellas placed in a rectangular duct of an attenuator were evaluated numerically and experimentally by Li et al. [13], showing that acoustic attenuation is primarily due to viscous and structural dissipation.

This article acoustically and aerodynamically evaluates attenuators with parallel acoustic panels in both linear and staggered topologies within a rectangular duct, considering simple, double, and triple baffled configurations. These configurations represent a downscaled version of a future noise attenuator to be incorporated into a turboengine test stand. Specialized literature on baffled noise attenuators provides calculation models that yield varying results. In this study, an analytical method for calculating the attenuation of a baffle attenuator is investigated alongside the finite element method and the results from both methods are compared with experimental data. The analyzed configurations are also evaluated from a gas dynamic perspective to determine pressure loss, using both an empirical method and the finite element method.

2. Noise Attenuation—Analytical Embleton Method

To identify a calculation model for the acoustic attenuation of a lamellar attenuator, both the analytical method developed by Embleton [14] and the finite element method using MSC Actran software were employed. The finite element method with Actran involves calculating acoustic propagation at each point in the grid, accounting for air impedance, reflections from solid and absorptive objects, propagation through porous materials, and free-field acoustic wave propagation.

The parameters necessary for calculating attenuation include the width of the lamella t, the distance between the baffles ly (which is the width of the air channel), and the baffle length L. These

 doi:10.20944/preprints202405.2135.v1

parameters are used to calculate the percentage of open area (POA [%]) of the attenuator, the ratio ly/λ (where λ is the wavelength), and the speed of sound in air c. Based on these data, the attenuation curves Aly from Figure 1 are consulted to complete the Embleton method [14].

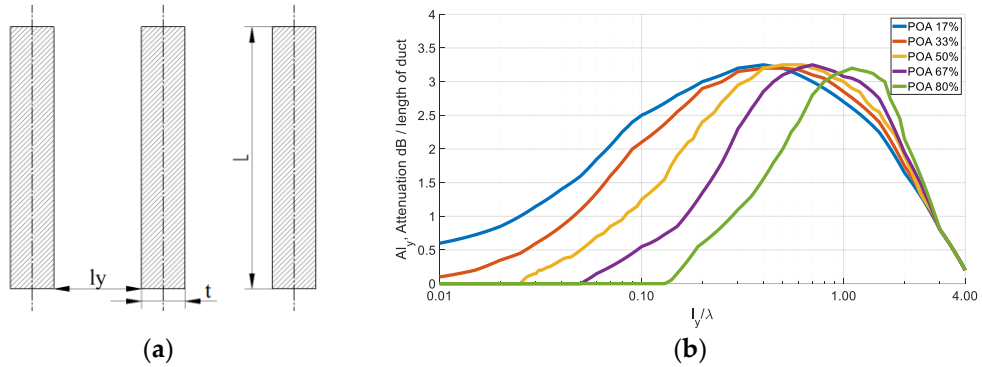

(**a**) (**b**)

Figure 1. Embleton method main parameters: (**a**) Schematic Presentation of the Attenuator; (**b**) graphs used for attenuation prediction (Embleton).

Based on the open area, the corresponding Al_y curve is selected and then multiplied by the ratio L/l_y, yielding the acoustic attenuation of the attenuator as described by Equation (1).

$$Attenuation = Al_y * \frac{L}{l_y} \text{ [dB]} \quad (1)$$

The open area is computed using the relation POA=$l_y/(l_y+t)$ × 100. For intermediate porosities, values from the graph can be interpolated. The frequency can be determined using Figure 1, where $f = (l_y/\lambda) \times (c/l_y)$.

The relationships for acoustic attenuation, as presented by Embleton [14] in the form of Equation (2), can be adjusted according to the airflow velocity between the baffles as follows:

$$Attenuation_{flow} = A(1 - 1.5 * M + M^2) \text{ [dB]} \quad (2)$$

where A is the noise attenuation without flow and M is the Mach number, and it is valid only for -0,3<M<0,3 [16].

The main disadvantage of this method is that the calculation model does not account for changes in the structural properties of the mineral wool, even though density is a known critical parameter that significantly influences acoustic attenuation by shifting the absorbed frequency. Another disadvantage is that the method neglects the properties of the perforated panel. Additionally, the calculation model is only applicable to simple attenuator geometries. However, the main advantage of this method is that it does not require complex software or significant computing resources, resulting in a short turnaround time for obtaining results.

Figure 2 presents an evaluation of the noise attenuation produced by a single-level attenuator and the influences of airflow through the baffles. It can be observed that for a high Mach number, the attenuation can decrease by more than 6 dB for the presented case. The Embleton method was utilized for calculating the noise attenuation and the flow correction, using Equation (1). The parameters of the attenuator were ly=0.1 m, t=0.1 m, and L=0.6 m.

 doi:10.20944/preprints202405.2135.v1

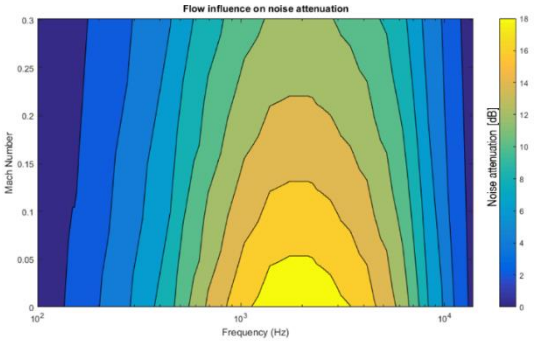

Figure 2. Noise attenuation of a single level attenuator depending the Mach number.

Flow-induced noise, also known as self-noise, is an inevitable consequence of fluid movement and is a crucial factor to consider in any system involving airflow. If self-noise becomes excessive, redesigning the baffle silencer becomes necessary, as other noise reduction methods might have limited effectiveness. In this study, an analytical method proposed by Munjal [17] is evaluated for the calculation of self-noise for the linear version of attenuators, and the results are compared with results from finite element method (FEM). Munjal's method is employed to estimate the acoustic power level generated by flow-induced noise in systems with baffles, such as noise attenuators. The Equation (3) is used in this method:

$$L_{w,self} = 10\log_{10}(2.16 \times 10^5 * U^{5.4} \cdot \frac{A_b}{(T+273)^{2.27}\left(\frac{POA}{100}\right)^4}) \text{ [dB]} \quad (3)$$

where A_b is the front area of the baffles [m²], T is the air temperature [°C] and POA is the percent of open area of the attenuator [%]. Self-noise is highly dependent on flow velocity. An increase in flow velocity will significantly impact the acoustic power level, as the power of flow-induced noise increases exponentially with the flow velocity.

3. Noise Attenuation—Finite Element Method

The validation of the Embleton model and the finite element method was conducted by comparing the results with experimentally obtained values. For this purpose, an experimental stand was constructed for testing lamellar attenuators. The finite element method involves creating a geometric model of the test bench, as presented in Chapter 3, meshing it, applying boundary conditions, and then conducting the acoustic analysis. The numerical scheme considers phenomena such as acoustic propagation in gaseous and porous media, acoustic reflections and absorptions, and the propagation of acoustic waves in a free field. Figure 3 presents the internal geometry of the test bench. To reduce computational time, a 2D simulation was performed. The applied boundary conditions are as follows: the blue line represents the boundary condition of acoustic pressure, with a pressure of 100 Pa applied along it, representing the acoustic source; the black lines represent the walls of the test bench, modeled as perfectly reflective surfaces; the red line represents the free field boundary condition, allowing the propagation of acoustic waves from inside the domain to the exterior without returning to the computational domain; the green lines represent the perforated panel with a porosity of of POA = 30%, hole diameter φ = 4 mm, panel thickness b = 0.5 mm, corresponding to the tested structure. The blue-colored surface inside the test bench represents the fluid domain with a sound speed c = 340 m/s and density ρ_0= 1.225 kg/m³, while the yellow domain represents the mineral wool for which was introduced a flow resistivity σ = 30000 Rayls/m, simulating a mineral wool density of approximately 80-100 kg/m³. In the acoustic analysis for calculating acoustic absorption and interior propagation through the porous material, the Delaney-Bazley calculation model was used. The red dots indicate the positions of the microphones used in the tests to evaluate the attenuation capacity of the silencers. The mesh, shown on the right side of Figure 3, is composed of rectangular elements with a maximum dimension of 8 mm, corresponding to a maximum analysis frequency of approximately 10 kHz.

 doi:10.20944/preprints202405.2135.v1

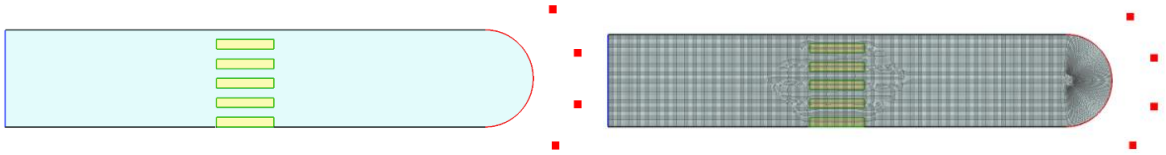

(**a**) (**b**)

Figure 3. Test bench geometry and computational grid: (**a**) geometry with boundary condition; (**b**) mesh.

The procedure for evaluating acoustic attenuation, both in numerical simulations and measurements, involves measuring the acoustic pressure at four points outside the test bench, positioned radially around the free end of the stand, and then logarithmically averaging them. The first measured configuration is without an acoustic baffle inside the duct, resulting in an average sound pressure $\overline{L_{p1}}$. This is followed by the introduction of baffles and subsequent measurement, resulting in an averaged sound pressure $\overline{L_{p2}}$. The difference between the two average noise levels represents the acoustic attenuation (insertion loss - *IL*) in dB of the tested configuration

$$IL = \overline{L_{p1}} - \overline{L_{p2}} \text{ [dB]} \quad (4)$$

The main advantage of this numerical method is its ability to model complex attenuator shapes and incorporate various parameters of the mineral wool and perforated panels. However, the computational cost increases with model complexity.

The primary disadvantage of this method is the significant computing resources required, particularly for 3D simulations. Additionally, creating the CAD model and, especially, the computational grid can be time-consuming.

4. Test Bench Description

To evaluate the attenuator's performance, a down-scaled model was tested under anechoic conditions. The testing stand, depicted in Figure 4, consists of a duct with a length of L_{duct} = 5.7 m and a rectangular cross-section with a width of l_{duct} = 1 m and a height of h_{duct} = 0.5 m . One end of the stand is closed, while the other remains open. At the closed end, inside the testing bench, an acoustic source (omnidirectional acoustic source Bruel & Kjaer 4292-L) was placed approximately 2 meters from the baffles, emitting pink noise in the frequency range of 50-16.000 Hz with an overall acoustic pressure level of approximately 125 dB, thus creating a strong diffuse field inside. At the open end, approximately 2 meters away from it, four microphones were placed according to Figure 4, and the acoustic spectra were logarithmically averaged. The stand was constructed from 18 mm thick chipboard panels with a density of 680-740 kg/m³. To stiffen the test bench and reduce acoustic transmission through its walls, the chipboard panels were doubled. To minimize unwanted noise, the tests were conducted inside the anechoic chamber of INCDT COMOTI.

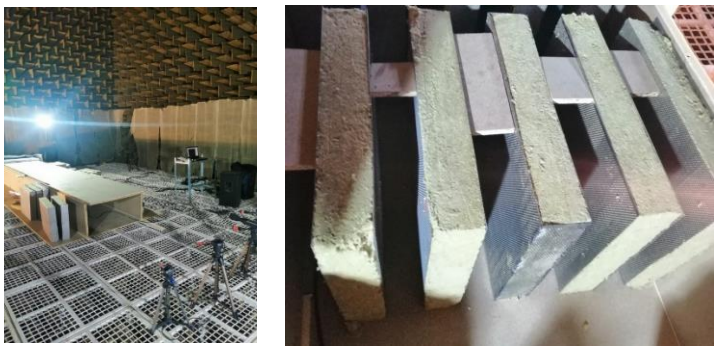

(**a**) (**b**)

Figure 4. Test bench inside the anechoic room and microphones location: (**a**)test bench in anechoic room; (**b**) Perforated sandwich panel baffle inside test bench.

 doi:10.20944/preprints202405.2135.v1

The baffled sandwich panels were made from basalt mineral wool with a density of 80 kg/m^3, and a steel perforated sheet with a percentage of openings of POA = 30%, hole diameters φ = 4 mm, and panel thickness b = 0.5 mm, baffle length L = 0.6 m, baffle height h = 0.5 m, baffle width l = 0.1 m, as presented in Figure 4b.

Specialized literature has shown that interleaving, or staggering, baffles lead to improved acoustic performance. Therefore, this study analyzed two attenuator models with staggered baffles and compared their acoustic attenuation results to linear baffle attenuators of the same total baffle length. Configurations II and IV, as well as configurations III and V, utilize the same total baffle length. However, in configurations IV and V, the baffles are staggered. Figure 5 presents schematic representations of the tested attenuator configurations. Configuration I consisted of a single attenuator section with parallel baffles.

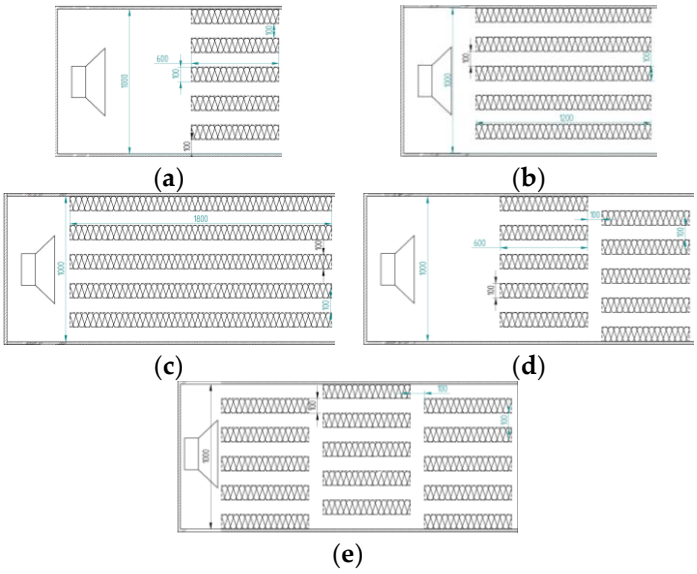

Figure 5. Drawings of the tested configurations: (**a**) Conf.I – single baffled_linear; (**b**) Conf. II – double baffled_linear; (**c**) Conf. III – triple baffled_linear; (**d**) Conf. IV – double baffled_staggered; (**e**) Conf. V – triple baffled_staggered.

The second configuration involved testing two baffle sections placed end-to-end. Similarly, the third configuration consisted of three baffle sections placed end-to-end. In contrast, the fourth configuration employed two staggered sections, while configuration V utilized three staggered baffle sections.

For all configurations, the distance between individual baffles and between staggered sections was maintained at l_s = 0.1 meters. Additionally, the exposed edges of the attenuators (those facing the acoustic waves) were covered with perforated panels, as presented in Figure 6.

Figure 6. Panel arranged in various topologies: (**a**) Conf.I – single baffled_linear; (**b**) Conf. II – double baffled_linear; (**c**) Conf. III – triple baffled_linear.

 doi:10.20944/preprints202405.2135.v1

In the present study, for the evaluation of configurations IV and V with staggered topology, an adaptation of Embleton's method is proposed to account for the intercalated (staggered) arrangement of the baffles. Since Embleton did not present a calculation method for staggered baffle configurations, we utilized the calculation for the linear version and modified the formula to address the differences between the calculated and measured results. The attenuation correction for the staggered baffle configuration includes three factors: l_c - distance addition correction, l_s - distance between two levels of baffles, and l_y - air channel width between baffles. It is considered that in the propagation path of the acoustic wave, in the case of intercalated lamellae, it travels a greater distance l_c, which is defined as follows:

$$l_c = n\frac{l_y}{\cos(\phi)} \text{ [m]} \quad (5)$$

where n is the number of baffled levels in staggered topology.

The following images illustrate the test results for various attenuator configurations. As shown in the graph in Figure 8, attenuation rapidly decreases at higher frequencies. This phenomenon, described by Embleton as the "beaming effect," occurs because high-frequency sound waves tend to travel directly through the gaps between the baffles. Consequently, they bypass the sound-absorbing material. Embleton suggests that high frequencies are not effectively absorbed due to this direct path. Instead of interacting with the absorptive material, the sound waves essentially travel the gaps with minimal influence, avoiding absorption and continuing to propagate.

Embleton proposes using of silencers with a staggered baffle arrangement, as shown in Figure 7. This design eliminates straight paths for sound waves to travel through the baffles, potentially leading to improved attenuation at higher frequencies. However, Embleton's research [14] is focused on parallel-baffled attenuators and did not provide prediction methods for staggered configurations. Consequently, this article proposes an adaptation of Embleton's method specifically for staggered topologies.

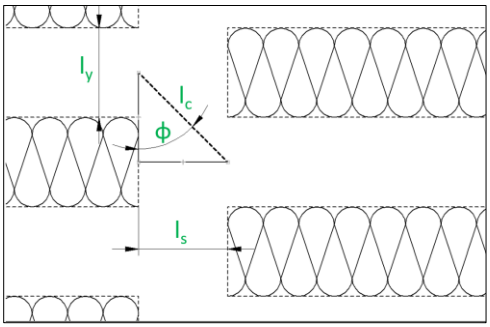

Figure 7. Attenuation correction in staggered baffles configuration.

5. Pressure Loss and Self-Noise Evaluation

The pressure loss, which refers to the reduction in air pressure as air flows through the duct system, was also evaluated for all configurations. This phenomenon occurs due to the friction and turbulence created by the internal surfaces and any acoustic treatments within the duct. Sound-absorptive materials like mineral wool and perforated steel sheets increase the roughness of the duct's internal surface, causing more friction between the air and the duct walls. Variations in duct cross-sectional area, designed to enhance noise attenuation by mitigating the beaming effect, can cause pressure changes and contribute to overall pressure loss. Excessive pressure drop can lead to additional noise, and compensatory higher flow speeds may result from the excessive pressure drop.

The effect of sound on rectangular plates placed in flow was studied by Welsh and Parker [18], who found that shear layers attach to the leading edge in the center of vorticity close to the boundary layer. Yu et al. [19] demonstrated the influence of rectangular geometries with different aspect ratios (ranging from 0.3 to 7) placed in flow through extensive simulation, showing their impact on the flow field. The influence of different geometries of edges on noise induced by flow was investigated by Mohany and Shoukry [20], who concluded that rectangular edge geometries with 0.5 aspect ratios

 doi:10.20944/preprints202405.2135.v1

show a significant increase in flow-excited acoustic pressure. Tang [21] investigated the sound produced by a low Mach vortex flow on a two-dimensional splitter, concluding that the sharp edge in the flow does not affect acoustic scattering.

The following Almgren formula [15] is used to calculate the pressure drop in a single baffled parallel attenuator with different length L of the baffles:

$$P = \frac{\xi \rho v_b^2}{2} + \frac{\lambda_{perf} L \rho v_b^2}{2 d_h} + \frac{\rho (v_b - v_0)^2}{2} \quad (6)$$

with local loss coefficient $\xi \approx 0.1$ and friction coefficient $\lambda_{perf} \approx 0.05$ (0.05 for smooth wall and 0.1 for rough walls) and d_h is the hydraulic diameter.

The first term from Equation (6) represents the pressure loss caused by the inlet and outlet effects of the flow through the baffles; the second term represents the pressure loss due to friction along the walls of the channel, and the last term is the pressure loss due to changes in air velocity. The pressure drop occurs at the beginning and at the exit of the baffle zone. Subsequently, the pressure drop for all linear configurations was analyzed using Equation (6) and compared with the results obtained from the Ansys Fluent software. Additionally, the staggered configurations were analyzed only with FEM. The boundary conditions introduced were: an airflow rate of 6.125 kg/s was defined at the inlet, corresponding to a speed of 10 m/s. The pressure loss was computed as the difference between the inlet and outlet total pressure. Based on the flow field, the noise power level inside the attenuator was computed using the Fluent acoustic module, which is based on Proudman's formula [22].

6. Results

6.1. Noise Assesment

The following section presents the acoustic results obtained from the test bench measurements and the application of the two previously described methods.

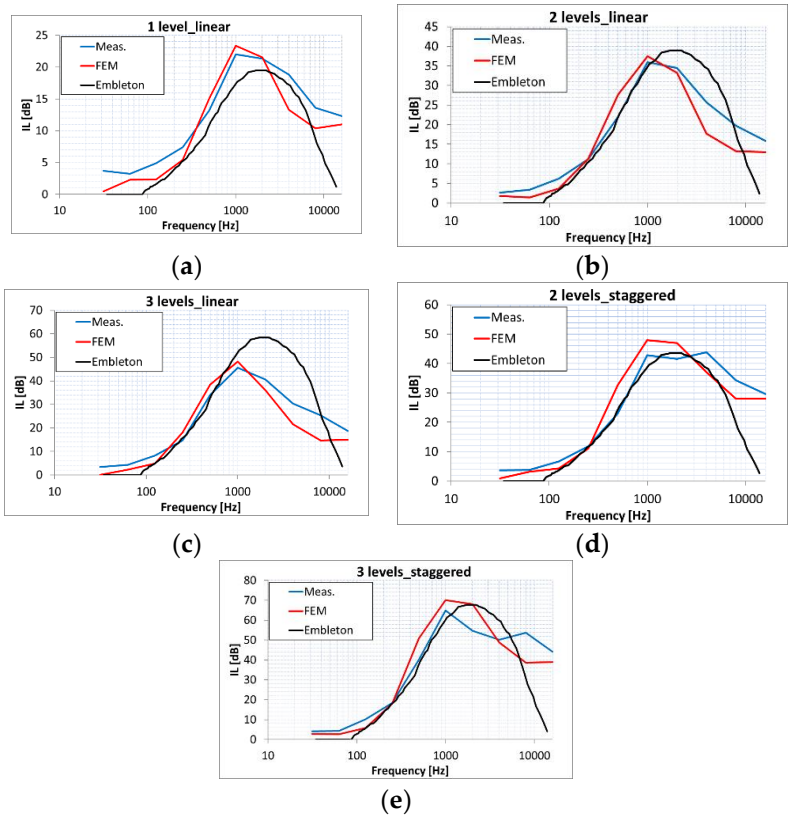

Figure 8. Comparative results between measurements and numerical modeling: (**a**) Conf.I – single baffled_linear; (**b**) Conf. II – double baffled_linear; (**c**) Conf. III – triple baffled_linear; (**d**) Conf. IV – double baffled_staggered; (**e**) Conf. V – triple baffled_staggered.

 doi:10.20944/preprints202405.2135.v1

Analyzing Figure 8, we observe that Embleton's method generally aligns with the attenuation curves. However, a sharp decrease in predicted attenuation becomes evident at higher frequencies. The experimental results demonstrate that even for configurations with linearly arranged baffles, high-frequency acoustic waves (>6 kHz) undergo significant acoustic attenuation; finite element numerical simulations capture acoustic attenuations at high frequencies very well.

Furthermore, both simulations and measurements show the maximum attenuation peak centered around 1.5 kHz, whereas the Embleton curve has its central frequency around 2 kHz. This shift of approximately 500 Hz is mainly due to the characteristics of the mineral wool from which the baffles are made. As previously mentioned, Embleton's method does not take into account changes in the density of the wool from which the baffles are constructed. For attenuator configurations with linearly arranged baffles, numerical simulations show a high degree of fidelity with the measurements. However, Embleton's method tends to overestimate attenuation as the length of the attenuator increases.

For the staggered baffle configuration, the finite element method predicts higher attenuation values than the measurements. This difference likely arises from two factors. Firstly, the CAD model assumes perfect baffle positioning, whereas real-world installations may involve slight deviations due to manufacturing tolerances or assembly processes. These deviations can introduce imperfections that reduce the effectiveness of the baffles. Secondly, high attenuation in staggered baffle configurations can make measurements susceptible to noise from collateral sound paths. This additional noise can contribute to lower measured attenuation values. One last aspect to note is that the numerical simulation achieves good correlation even at low frequencies, which are very important, especially in applications where such attenuators are used.

Figure 9 presents a comparison graph of the average insertion loss for all configurations investigated in this study. Since the primary focus of this research was to identify the optimal configuration for a sound attenuator in a turboengine test stand, a three-baffle staggered arrangement emerges as the most suitable choice.

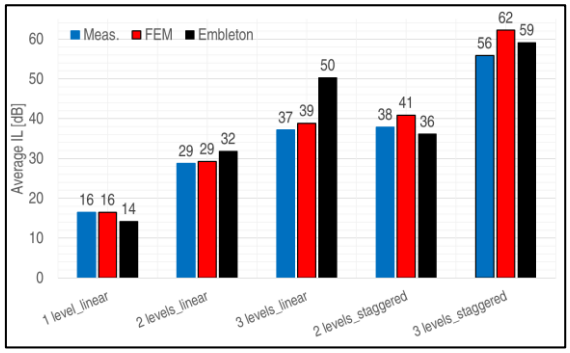

Figure 9. Averaged Insertion Loss for the analyzed configurations of attenuator.

Figure 10 presents a comparison of sound pressure levels obtained using Actran software for a linear three-baffle configuration and a staggered three-baffle configuration. The results visually demonstrate a more attenuated acoustic field within the staggered baffle variant compared to the linear one. Consequently, the staggered configuration appears to be a more suitable choice for the final test stand application. The acoustic fields reveal another important consideration: even though all channels have a width of 0.1 meters, the marginal channel with one reflective wall allows for sound leakage. Therefore, in the final application, it's crucial to ensure that the duct walls are acoustically treated.

 doi:10.20944/preprints202405.2135.v1

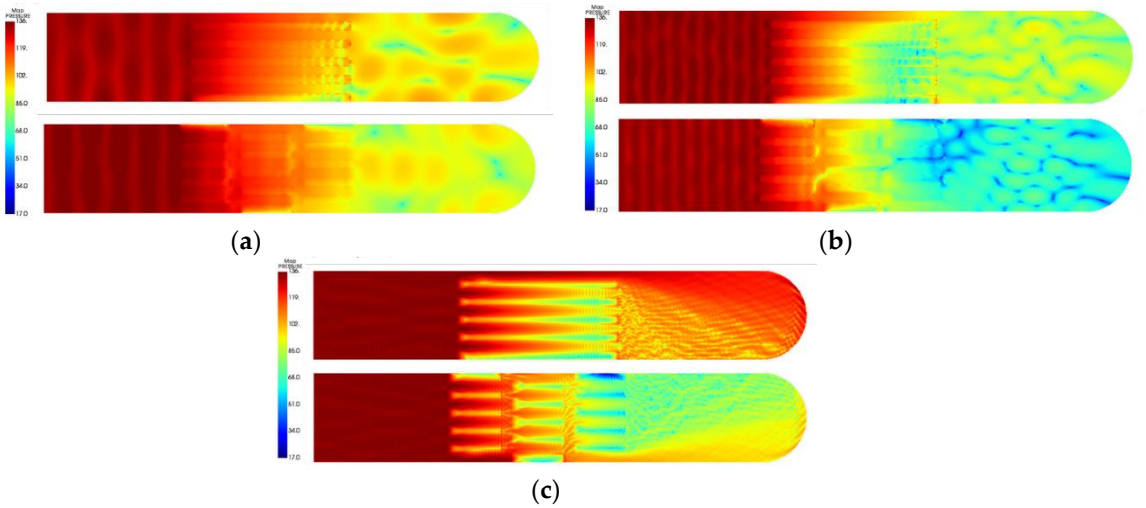

Figure 10. Acoustic field inside test bench - sound pressure level [dB]: (**a**)500 Hz; (**b**)1000Hz; (**c**) 5000Hz.

6.2. Pressure Loss and Self-Noise Assesment

Table 1 presents the pressure loss for each configuration that was analyzed by using Algrem [15] analytical method.

Table 1. Pressure loss for each configuration.

Configuration	Pressure loss [Pa]	
	Analytic	FEM
Conf. I – single baffled_linear	124	164
Conf. II – double baffled_linear	154	175
Conf. III – triple baffled_linear	184	191
Conf. IV – double baffled_staggered	-	446
Conf. V – triple baffled_staggered	-	737

Linear configurations exhibit lower pressure losses compared to staggered configurations. Staggered configurations generate significantly higher-pressure losses due to the increased flow complexity and stronger interactions between the jets and deflector surfaces.

In Figure 11 the pressure and velocity field inside the attenuator are presented.

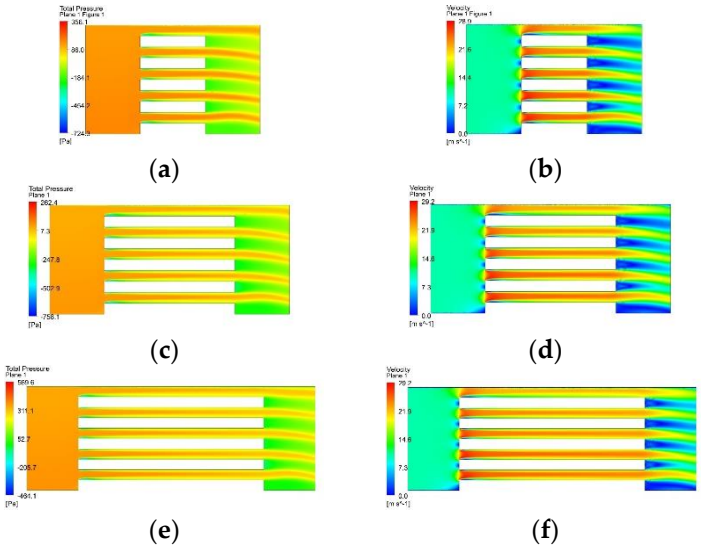

 doi:10.20944/preprints202405.2135.v1

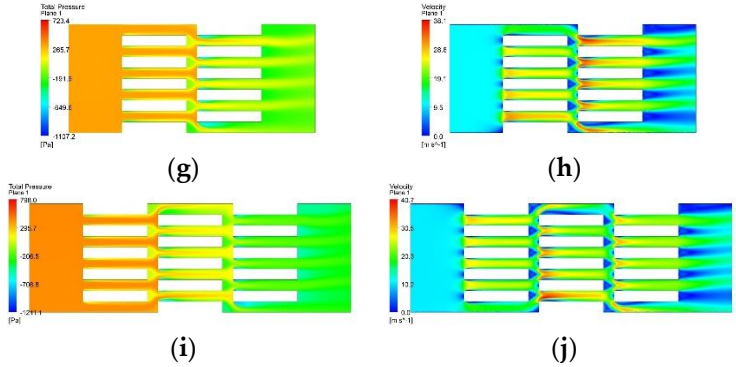

Figure 11. Flow fields inside the attenuator: (**a**)pressure field – conf I; (**b**) velocity field – conf I; (**c**)pressure field – conf II; (**d**) velocity field – conf II; (**e**)pressure field – conf III; (**f**) velocity field – conf III; (**g**)pressure field – conf IV; (**h**) velocity field – conf IV; (**a**)pressure field – conf V; (**b**) velocity field – conf V.

The single baffled linear configuration shows the lowest pressure loss among all configurations analyzed. The close agreement between Almgren's and FEM results (124 Pa vs. 164 Pa) suggests a reliable estimation of pressure loss for this simple configuration. Adding a second baffle in a linear arrangement increases the pressure loss slightly compared to the single baffled configuration. The results from Almgren and FEM are again quite close (154 Pa vs. 175 Pa), indicating a consistent and predictable increase in pressure loss due to the additional baffle. Introducing a third baffle continues to increase the pressure loss, but the increase is not as significant as might be expected. The close match between Almgren and FEM results (184 Pa vs. 191 Pa) shows that the linear addition of baffles has a diminishing effect on increasing pressure loss. The staggered configuration with two baffles results in a significant increase in pressure loss compared to the linear configurations. The FEM analysis shows a pressure loss of 446 Pa, which is substantially higher than the double baffled linear configuration. This indicates that the staggered arrangement causes more turbulence and resistance to airflow. The staggered configuration with three baffles shows the highest-pressure loss at 737 Pa, as per the FEM analysis. This configuration introduces the most significant turbulence and obstruction to airflow, leading to the highest energy loss among all configurations analyzed.

Square-edged baffles have a significant negative impact on airflow or fluid flow. Their sharp-edged design causes flow separation at the deflector inlet, leading to the formation of recirculation zones and turbulence downstream of the deflector. This separation and recirculation contribute to energy losses in the form of heat and increase pressure losses. In a staggered configuration, deflectors are arranged in a way that forces the flow to follow a zigzag path. This creates multiple points of flow acceleration and deceleration, each point contributing to additional pressure losses, similar to the effect of steps. In addition to increasing pressure losses, the turbulence and recirculation zones generated by square-edged deflectors and staggered configurations have another important effect: noise generation.

Turbulence creates vortices and rapidly changing pressure fluctuations, which are significant sources of noise. These fluctuations are transmitted through the air as sound waves, perceived as a disturbing noise. The more intense the turbulence, the higher the generated noise level. Square-edged deflectors promote flow separation and the formation of strong turbulence, leading to significantly higher noise.

The acoustic field inside each analyzed configuration is presented in Figure 12.

 doi:10.20944/preprints202405.2135.v1

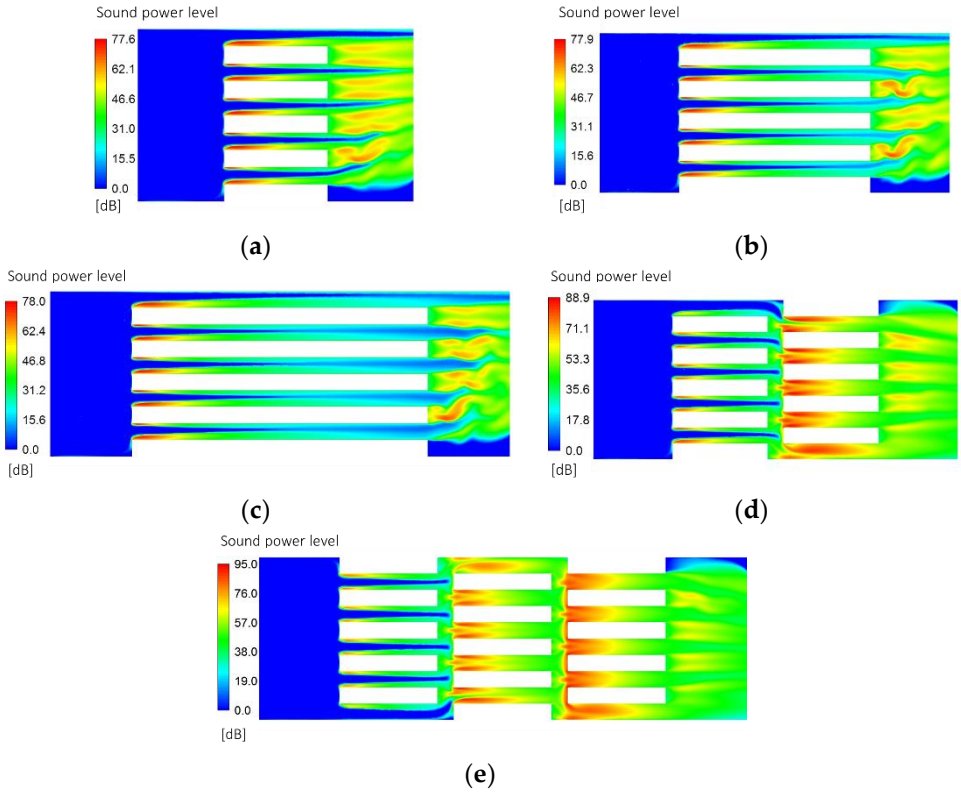

Figure 12. Noise induced by the flow inside the attenuator – Acoustic Power Level [dB]: (**a**) Conf.I – single baffled_linear; (**b**) Conf. II – double baffled_linear; (**c**) Conf. III – triple baffled_linear; (**d**) Conf. IV – double baffled_staggered; (**e**) Conf. V – triple baffled_staggered.

Figure 12 illustrates the acoustic field and noise levels for different deflector configurations. The figure supports the following observations: The sharp-edged design causes flow separation at the deflector inlet, leading to recirculation zones and turbulence downstream, which generate noise. For linear attenuator versions (Conf. I, Conf. II, Conf. III), the sound power level of the acoustic sources does not show significant increases, the primary noise sources being located near the leading edge of the baffle. In staggered attenuator variants (Conf. IV, Conf. V), the interaction of the upstream channel air flow with the leading edge of the downstream baffle amplifies the phenomenon downstream.

Table 2. Self-noise for each configuration – Sound power level computed with FEM.

Configuration	Sound power level [dB]
Conf.I – single baffled_linear	77.6
Conf. II – double baffled_linear	77.9
Conf. III – triple baffled_linear	78.0
Conf. IV – double baffled_staggered	88.9
Conf. V – triple baffled_staggered	98.0

According to Munjal [17] (Equation (3)), the resulted self-noise is 79.7 dB for single, double and triple baffle, because in this formula the length of the baffle is not included. In comparation, the FEM results are simillar with analytic ones, but more reliable to be used in practice.

This study primarily aimed to evaluate various topologies of lamellar attenuators intended for use in turboengine test stands, mainly from an acoustic perspective and under static conditions. Although some flow conditions were introduced in the evaluation, the study did not include testing in actual airflow. Future research endeavors should focus on conducting acoustic simulations under flow conditions. Additionally, optimizing the geometry of the attenuators by incorporating rounded leading and trailing edges on baffles could further enhance their performance.

 doi:10.20944/preprints202405.2135.v1

7. Conclusion

This paper has undertaken a comprehensive preliminary analysis of a sound attenuator module used for turboengine test stands, addressing a critical need in the field of noise management for high-performance turboengine testing environments. Through an examination of material parameters, design configurations, and integration techniques, we have provided a detailed framework for an effective procedure for projecting noise attenuators. While the study primarily focused on the static acoustic behavior of an attenuator, considerations were made on flow dynamics, assessing the attenuation at different Mach numbers, pressure drop, and self-generated noise aspects to provide a broader perspective in choosing the best design configuration.

The study explored various calculation methods for evaluating noise reduction in both linear and staggered baffles, using a scaled-down model of an attenuator. Analytical methods and advanced computational techniques such as finite element analysis were employed, along with an adapted and modified Embleton calculation method for staggered baffle configurations, to predict the acoustic performance of various attenuator designs. It was concluded that the Embleton method, while widely used, tends to offer excessive and unrealistic values for linear configurations, prompting the need for modification, especially for staggered configurations. These simulations were complemented by experimental validations, confirming the reliability and accuracy of the predicted outcomes. Embleton's method generally aligned with the attenuation curves, although a noticeable decrease in predicted attenuation was observed at higher frequencies. Experimental data revealed significant acoustic attenuation even for configurations with linearly arranged baffles, particularly at frequencies exceeding 6 kHz. However, a discrepancy was noted between the central frequencies of the attenuation peaks obtained from measurements and Embleton's method, primarily due to the method's inability to account for variations in the density of the mineral wool used in the baffles.

Finite element numerical simulations exhibited a high degree of fidelity with experimental measurements, especially at high frequencies. For linearly arranged baffles, the simulations accurately reflected the measured attenuation levels. However, Embleton's analytic method tended to overestimate attenuation as the length of the attenuator increased. In contrast, staggered baffle configurations predicted higher attenuation values compared to measurements. This disparity was attributed to assumptions made in the CAD model regarding perfect baffle positioning, as well as the introduction of noise from collateral sound paths in staggered configurations. The comparison graph of average insertion loss indicated that a three-baffle staggered arrangement emerged as the most suitable choice for turboengine test stand applications. Additionally, comparisons of sound pressure levels revealed that the staggered configuration provided more attenuated acoustic fields compared to linear configurations.

Pressure loss assessments demonstrated that linear configurations generally exhibited lower pressure losses compared to staggered configurations, which is also obvious. Staggered arrangements induced higher-pressure losses due to increased flow complexity and interactions between jets and deflector surfaces. Acoustic field analyses highlighted the impact of sharp-edged deflectors on flow separation, turbulence generation, and subsequent noise generation. Staggered configurations exacerbated these effects, leading to significantly higher noise levels compared to linear arrangements.

Overall, this study provided valuable insights into the acoustic and aerodynamic performance of lamellar attenuators for turboengine test stand applications. Future research should focus on conducting acoustic simulations under flow conditions and optimizing attenuator geometries to further enhance performance.

Author Contributions: Conceptualization, L.C. and M.D.; methodology, M.D.; software, M.D.; validation, L.C., M.D.; formal analysis, L.C.; investigation, L.C.; data curation, X.X.; writing—original draft preparation, L.C., M.D.; writing—review and editing, L.C., M.D.; visualization, X.X.; supervision, X.X. All authors have read and agreed to the published version of the manuscript.

Funding: This work was carried out through the Nucleu Program within the National Plan for Research, Development, and Innovation 2022-2027, conducted with the support of MCID, project no. PN23.12.01.01.

 doi:10.20944/preprints202405.2135.v1

Institutional Review Board Statement: Not applicable.

Informed Consent Statement: Not applicable.

Data Availability Statement: MDPI Research Data Policies" at https://www.mdpi.com/ethics.

Acknowledgments: The data presented and analyzed in this report were obtained with the help of INCDT COMOTI's Research and Experiments Center in the field of Acoustic and Vibrations staff and facility and the work was carried out through the anechoic chamber and measurement equipment.

Conflicts of Interest: The authors declare no conflicts of interest. The funders had no role in the design of the study; in the collection, analyses, or interpretation of data; in the writing of the manuscript; or in the decision to publish the results.

References

1. Bies D., Hansen C., *Flow resistance information for acoustical design.* Applied Acoustic, 1980.
2. Wang C., Li C. and Hunag L. *Realization of a broadband low-frequency plate silencer using sandwich plates*. Journal of Sound and Vibration, 2008.
3. Erkan D., *Duct Acoustics. Fundamentals and Applications to Mufflers and Silencers*, Cambridge University Press, 2021.
4. Sumit S., Kumbhar S. and Goilkar S., *Acoustics and Flow Field Analysis of Perforated Muffler Design*, International Journal of Engineering Development and Research, 2014.
5. Yu X. and Cheng L. *Duct noise attenuation using reactive silencer with various internal configurations*. Journal of Sound and Vibration, 2015.
6. Wang H., Vardy A. E. and Dubravka Pokrajac, *Pressure radiation from a perforated duct exit region*. Journal of Sound and Vibration, 2015.
7. Zhou C.W., Lainé J.P., Ichchou M.N. and Zine A.M.. *Numerical and experimental investigation on broadband wave propagation features in perforated plates.* Mechanical Systems and Signal Processing, 2016.
8. Williams P., Kirby R., Hill J., Åbom M. and Malecki C..*Reducing low frequency tonal noise in large ducts using a hybrid reactive-dissipative silencer*. Applied Acoustics, 2018.
9. Terashima F. J. H., de Lima K. F., Barbieri N., Barbieri R. and Filho N. L. M. L.. *A two-dimensional finite element approach to evaluate the sound transmission loss in perforated silencers.* Applied Acoustics, 2022.
10. Kalita U. and Singh M. *Acoustic performance analysis of muffler by varying sound absorption materials*. MaterialsToday, 2023.
11. Su X. *Acoustics of parallel baffles muffler with Micro-perforated panels*. KTH Aeronautical and Vehicle Engineering, 2011.
12. Liu. L, Qio Y., Hao Z. and Sheng X. *A modified time domain approach for calculation of noise reduction and acoustic impedance of intake duct system,* Applied Acoustics, 2020
13. Li K., Nenning B., Perrey-Debain E. and Dauchez N. *Poroelastic lamellar metamaterial for sound attenuation in a rectangular duct.* Applied Acoutics, 2021
14. Embleton T. Mufflers in Beranek L. *Noise and Vibration control*. Insitute for Noise Control Engeneering, 1971, pp. 362-405.
15. Bogdanovici D. *Calculation methods for predicting attenuation of parallel baffle type silencers*. Chalmers University of Technology, 2014.
16. Ray E.. *Industrial noise series VII*; Absorptive silencer design. Universal, 2010.
17. Munjal M. L. *Acoustics of Ducts and Mufflers with Application to Exhaust and Ventilation System Design*., Wiley-Interscience, 1987.
18. Parker R. amd Welsh C. *Effects of sound on flow separation from blunt flat plates,* International Journal of Heat and Fluid Flow, 1983
19. Yu D., Butler K., Kareem A., Glimm J. and Sun J. *Simulation of the Influence of Aspect Ratio on the Aerodynamics of Rectangular Prisms*, Journal of Engineering Mechanics, 2012
20. Shoukry A. and Mohany A. *Characteristics of the flow-induced noise from rectangular rods with different aspect ratios and edge geometry.* Journal of Fluids and Structures, 2023
21. Tang S. K. *Duct sound produced by vortex flow over a splitter plate*, Journal of Sound and vibration, 2022
22. Proudman I. *The generation of noise by isotropic turbulence*, Proceedings of the Royal Society of London, Vol. 214, No. 1116 , pp. 119-132 , 1952